Available online at www.sciencedirect.com
SCIENCE DIRECT
ELSEVIER
Journal of the European Ceramic Society 26 (2006) 2761–2767
ECERS
www.elsevier.com/locate/jeurceramsoc

# Investigation on crystallization and influence of $Nd^{3+}$ doping of transparent oxyfluoride glass-ceramics

Yunlong Yu, Daqin Chen, Yao Cheng, Yuansheng Wang *, Zhongjian Hu, Feng Bao

*The State Key Laboratory of Structural Chemistry, Fujian Institute of Research on the Structure of Matter, Chinese Academy of Sciences; Graduate School of the Chinese Academy of Sciences, Fuzhou, Fujian 350002, China*

Received 7 February 2005; received in revised form 18 May 2005; accepted 24 May 2005
Available online 20 July 2005

**Abstract**

$Nd^{3+}$ doped transparent oxyfluoride glass-ceramics containing $LaF_3$ nano-crystals were prepared by melt quenching. Differential thermal analysis (DTA) showed that the addition of $NdF_3$ decreased the $LaF_3$ crystallization temperature. The kinetics studies indicated that the crystallization was a diffusion-controlled growth process with zero nucleation rate for the whole process. $LaF_3$ crystallization activation energy and crystalline size as the function of $NdF_3$ doping lever exhibit the closely related evolutions. For the crystallized samples, transmission electron microscopy (TEM), X-ray diffraction (XRD), energy dispersive X-ray spectroscopy (EDS) and absorption spectroscopy experiments evidenced the homogeneous distribution of spherical $LaF_3$ nano-crystals (10–20 nm) with the incorporation of $Nd^{3+}$ ions in the lattice among the oxide glassy matrix, which is important for obtaining desirable luminescent performance of the material.
© 2005 Elsevier Ltd. All rights reserved.

*Keywords:* Glass-ceramics; Microstructure; $Nd^{3+}$ doping

## 1. Introduction

Rare-earth doped transparent oxyfluoride glass ceramics, in which rare-earth ions selectively incorporated into the fluoride nano-crystals immersed in an oxide glassy matrix, can offer excellent luminescent properties due to the combination of the advantages of both fluorides and oxides: low phonon energy environment of fluoride crystalline for luminescent ions, and good mechanical and chemical properties of oxide matrix.[1,2] This new material has attracted great attention in the continuous research for the novel optoelectrionic devices.

$Nd^{3+}$ is one of the most widely studied luminescent ions, and $Nd^{3+}$ doped crystalline,[3] glass[4] and ceramics[5] have been applied in many fields. Compared with other lanthanide ions, however, only a few works have been devoted to the research on $Nd^{3+}$ doped transparent oxyfluoride glass-ceramics. It was reported that $Nd^{3+}$ ions are difficult to be incorporated into crystalline phase for oxide glass-ceramics,[6,7] and $Nd^{3+}$ doped oxyfluoride glass-ceramics containing $Pb(Cd)F_2$ are susceptible to proceed spontaneous devitrification during glass preparation which was not observed when doping the same glass matrix with $Er^{3+}$, $Eu^{3+}$, $Yb^{3+}$, or $Tm^{3+}$ ions.[8] The $LaF_3$ crystals are considered to be a more suitable host for rare-earth ions than $Pb(Cd)F_2$ because the solid-solubility of rare-earth ions can be superior, owing to the similar ionic radius and the same valence for La and other rare-earth ions.[2,9,10] In this work, we studied the crystallization behavior and the influence of $Nd^{3+}$ doping of oxyfluoride glass-ceramics containing $LaF_3$ crystals.

## 2. Experimental

The glass-forming compositions are $41.2SiO_2$-$29.4Al_2O_3$-$17.6Na_2CO_3$-$11.8LaF_3$-$xNdF_3$ ($x = 0$, 0.5,

* Corresponding author. Tel.: +86 591 83705402; fax: +86 591 83705402.
*E-mail address:* yswang@fjirsm.ac.cn (Y. Wang).

0955-2219/$ – see front matter © 2005 Elsevier Ltd. All rights reserved.
doi:10.1016/j.jeurceramsoc.2005.05.002

1, 2, 3 and 4) in mol%, accordingly, the samples are named in the following text as samples 1–6, respectively. High purity reagents (≥3N) were used as the starting materials. The mixed batches were melted in a covered platinum crucible under the air atmosphere at 1350 °C for 1 h. The melt was then poured into a copper mold to proceed rapid quenching. The obtained glassy samples with 3–4 mm thickness were annealed to release the stress at the temperatures 20–30 °C below the glass transition temperatures ($T_g$) determined by DTA (NETZSCH-TA4). The annealed samples were then cut into about 2 cm square coupons. To investigate the crystallization microstructure, the samples were heat-heated at 10 °C/min to 650 °C or 670 °C, and held for 8 h, respectively.

The non-isothermal method was employed to evaluate the kinetics of crystallization. DTA measurements were carried out in air at the heating rates of 5, 10, 15, 20 and 25 °C/min, respectively. The samples used were bulk glass pieces (5–10 mg). To identify the crystallization phase, XRD analyses were carried out with a powder diffractometer (DAMX2500), using Cu K$\alpha_1$ as the radiation, at 40 kV and 100 mA. The $2\theta$ scan range was 5°–85°, with a step size of 0.05° and a resolution of 0.01°. The microstructure of samples was analyzed by TEM and high-resolution TEM (HRTEM) with JEM-2010 transmission electron microscope equipped with EDS and CCD imaging systems and operated at 200 kV. TEM specimens were prepared by dispersing fine power grinded from bulk sample in ethanol, followed by ultrasonic agitation, and then depositing onto a carbon enhanced copper. Optical absorption spectra were recorded by an UV-near-infrared spectrophotometer (Lambda900) at room temperature to monitor the changes of the environmental structure of the $Nd^{3+}$ ions.

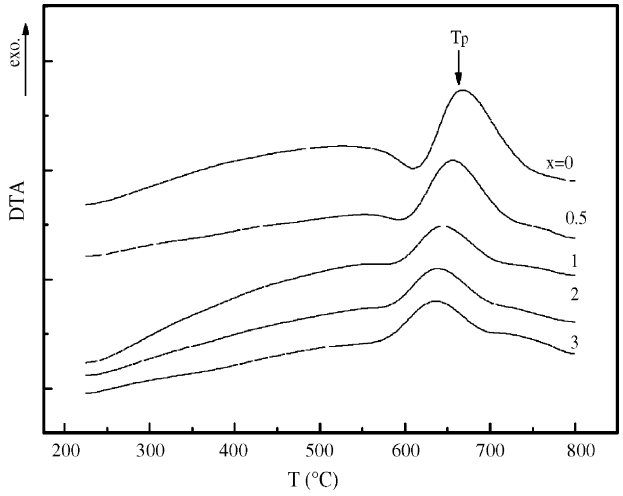


Fig. 1. DTA curves of the as-made samples doped with × mol% of $NdF_3$.

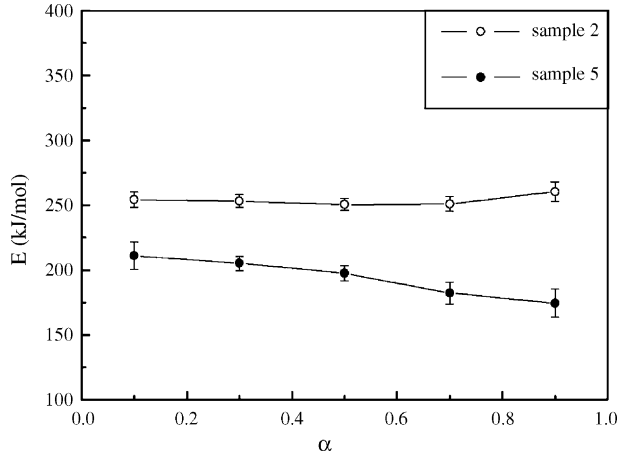


Fig. 2. The apparent crystallization activation energy for samples 2 and 5 estimated by Ozawa's equation as a function of fractional conversion. Lines are drawn as guides for the eye.

## 3. Results and discussions

### 3.1. Thermal analysis

The as-made samples 1–5 were visually transparent, appearing blue-purple due to $Nd^{3+}$. Sample 6 was translucent due to spontaneous devitrification during melt quenching revealed by HRTEM observation. Therefore, only samples 1–5 were further investigated in this work.

The DTA curves for the as-made samples with different $NdF_3$ content are shown in Fig. 1. A unique exothermic peak appears for all the curves, indicative of the $LaF_3$ crystallization from the glass matrix confirmed by XRD analysis. With increasing of $NdF_3$ doping, the peak position shifts to the lower temperature side, e.g. from 667 °C for sample 1 to 642 °C for sample 5, indicating the hastening of crystallization onset. For as-made sample 1, the nucleus of crystallization was generated by the over-melted liquid itself,[11] and the nucleation was homogenous. For the $NdF_3$ doped samples, it is possible that the impurities, i.e. $NdF_3$, acted as the seeds to prompt the crystallization based on heterogeneous nucleation at a lower temperature.

Table 1
Theoretical kinetic model functions

| Symbol | Equation | Mechanism | $f(\alpha)$ |
|---|---|---|---|
| JMA | Johnson-Mehl-Avrami | Random nucleation and growth or diffusion-controlled growth | $(1-\alpha)[-\ln(1-\alpha)]^{n-1/n}$ |
| $A_1$ | Prout-Tompkins law | Ramiform nucleation induced by the interference of growing nucleus | $\alpha(1-\alpha)$ |
| $B_2$ | | Phase boundary reaction, cylindrical symmetry | $\alpha(1-\alpha)^{1/2}$ |
| $D_8$ | Wert-Zener | Diffusion-controlled continuous precipitation | $\alpha^{1/3}(1-\alpha)$ |

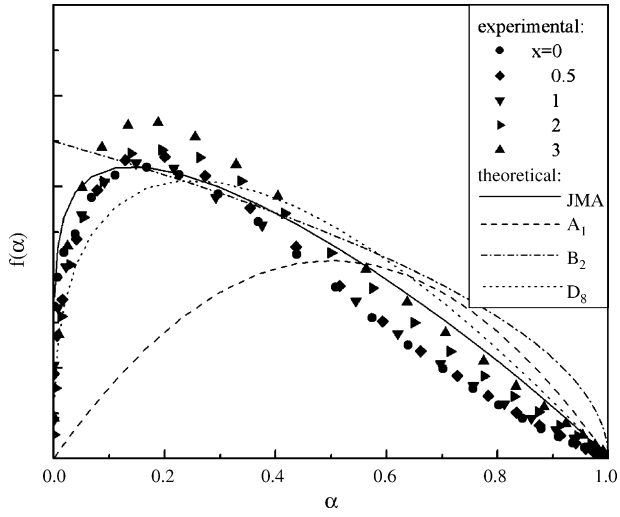


Fig. 3. The experimental data of $f(\alpha)$ for samples doped with different content of $NdF_3$ and the various theoretical $f(\alpha)$ curves based on different mechanisms.

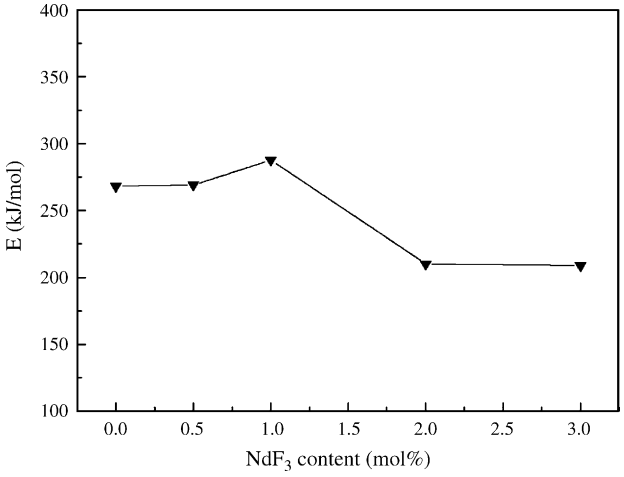


Fig. 4. Evolution of the apparent crystallization activation energy of $LaF_3$ estimated by Ozawa's equation as a function of the $NdF_3$ content. Lines are drawn as guides for the eye.

The crystallization kinetics of amorphous solids has been extensively studied by thermal analysis, such as DTA or DSC. The equation of the crystallization kinetics could be usually expressed in the following form:

$$\frac{d\alpha}{dt} = A \exp\left(\frac{-E}{RT}\right) f(\alpha) \quad (1)$$

Table 2
The Avrami exponent $n$ estimated by Ozawa's equation for the samples doped with different content of $NdF_3$

| $T$ (K) | $x$ | | | | |
|---|---|---|---|---|---|
| | 0 | 0.5 | 1 | 2 | 3 |
| 908 | 1.50 | 1.49 | 1.12 | 1.03 | 1.14 |
| 913 | 1.48 | 1.44 | 1.10 | 1.08 | 1.11 |
| 918 | 1.42 | 1.40 | 1.13 | 0.92 | 1.12 |
| Average value | 1.47 | 1.44 | 1.12 | 1.01 | 1.12 |

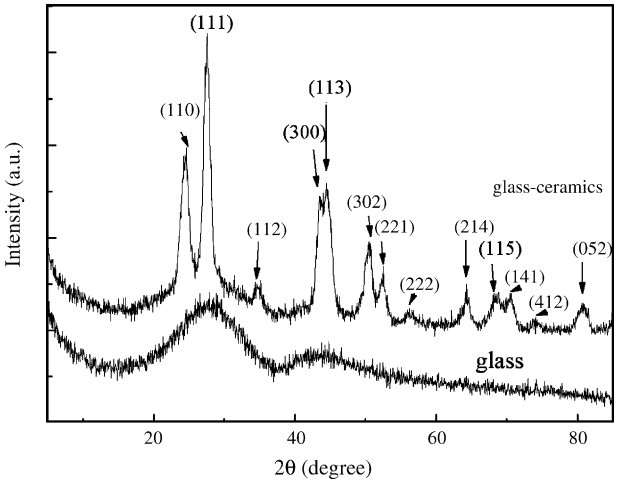


Fig. 5. XRD patterns of sample 3 in the states of as-made and heat-treated at 650 °C, respectively.

Eq. (1) can be rewritten as:

$$f(\alpha) = \frac{d\alpha}{dt} A^{-1} \exp\left(\frac{E}{RT}\right) \quad (2)$$

where $\alpha$ is the fractional conversion, $d\alpha/dt$ the reaction rate, $A$ the pre-exponential factor, $E$ the apparent crystallization activation energy, $R$ the gas constant, $T$ the temperature and $f(\alpha)$ the kinetic model function. Several kinetic model functions from the literatures[12,13] are listed in Table 1. The value of $E$ at a fixed fractional conversion can be evaluated by Ozawa's non-isothermal method[14,15]:

$$\frac{d[\ln(\beta)]}{d(1/T_\alpha)} = -\frac{E}{R} \quad (3)$$

where $\beta$ is the heating rate, $T_\alpha$ the temperature corresponding to the fixed fractional conversion $\alpha$. The apparent crystallization activation energies for samples of different $NdF_3$ content were obtained from the slopes of Eq. (3). Fig. 2 shows the activation energies for samples 2 and 5 as a function of frac-

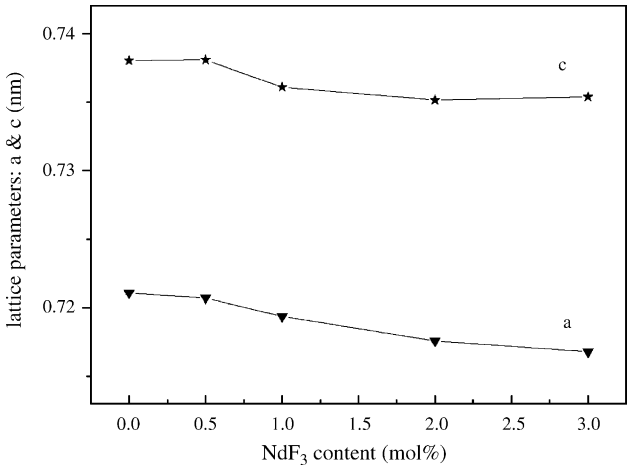


Fig. 6. Evolution of the lattice parameters ($a$ and $c$) of hexagonal $LaF_3$ as the function of $NdF_3$ content. Lines are drawn as guides for the eye.

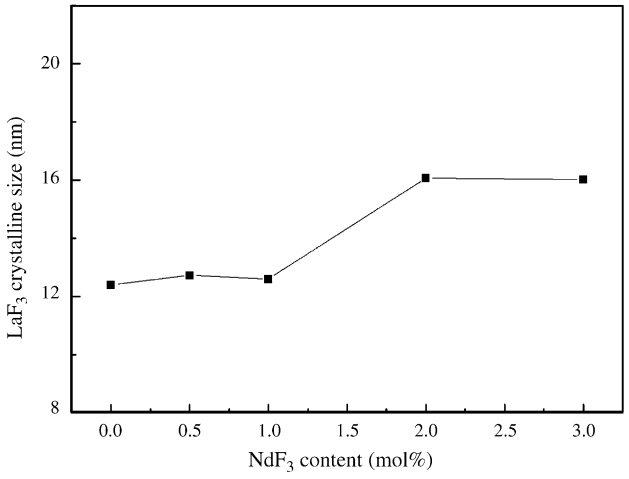


Fig. 7. Evolution of the mean crystalline size of $LaF_3$ in the samples heat-treated at 650 °C as a function of the $NdF_3$ content. Lines are drawn as guides for the eye.

tional conversion $\alpha$. Within the limits of the experimental errors, the activation energy of sample 2 or 5 is basically the same for different fractional conversions, which revealed that the crystallization mechanism is invariable for the whole crystallization process. The curves of $f(\alpha)$ as a function of the fractional conversion $\alpha$ can be calculated from Eq. (2). The theoretical curves corresponding to various mechanism models (shown in Table 1) and the experimental data transformed from Eq. (2) are shown in Fig. 3, which revealed that only the JMA model is in agreement with the experimental results.

The average values of $E$ for the whole crystallization process as a function of the $NdF_3$ content are shown in Fig. 4. It is verdict from Fig. 4 that $E$ for samples with low ($\leq$1 mol%) $NdF_3$ content did not change remarkably compared to that of sample 1. However, it decreased abruptly when $NdF_3$ content reached 2 mol%. When $NdF_3$ content was further increased to 3 mol%, it kept unchanged again.

Avrami exponent, $n$, which is a parameter related to the nucleation and growth mechanism and dimensionality of crystal, can be obtained by Ozawa's equation[14]:

$$\left.\frac{\mathrm{d}\{\ln[-\ln(1-\alpha)]\}}{\mathrm{d}\,\ln(\beta)}\right|_T = -n \tag{4}$$

where $\alpha$ is the fractional conversion at a fix temperature $T$. Almost all the Avrami exponents calculated from the slop of

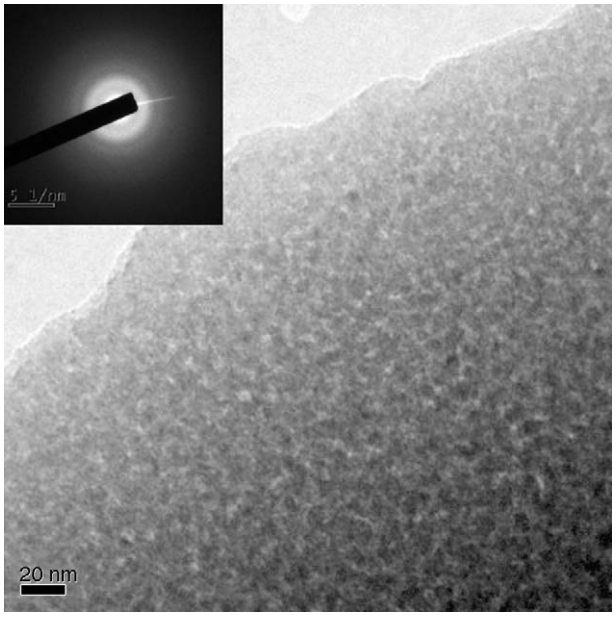


Fig. 8. TEM bright field image for as-made sample 3, the inset shows the corresponding electron diffraction pattern.

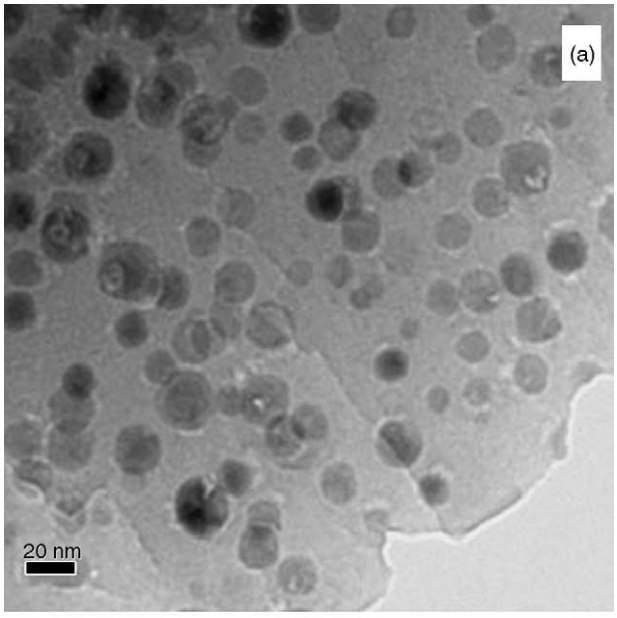


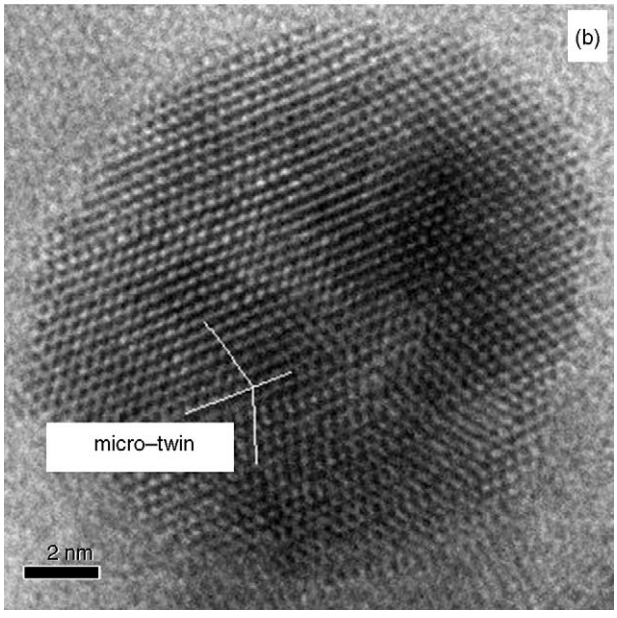


Fig. 9. TEM micrographs of sample 1 heat-treated at 670 °C. (a) Bright field image showing the distribution of $LaF_3$ crystallites, and (b) high-resolution image of a crystallite embedded in the glassy matrix.

the plots of Eq. (4) are in the range of 1.0–1.5, as listed in Table 2.

The good agreement between the experimental data and the theoretical curve of the JMA model implies that the crystallization of the samples follows the JMA kinetics model. The values of activation energy (ranging from 208.1 to 278.7 kJ/mol for samples with different $NdF_3$ doping) and Avrami parameter further indicate the crystallization for all samples being a diffusion-controlled growth process with zero nucleation rate.[16] The decreasing of crystallization activation energy when $NdF_3$ content reached 2 mol% is probably due to the seeding effect of $NdF_3$ and the non-bridging function of fluorine anions which reduces the network connectivity and structural stability of oxide glassy matrix.[17] The later is also responsible for the experimental phenomena that melt viscosity reduced with increasing of $NdF_3$ content during preparation of the glass sample.

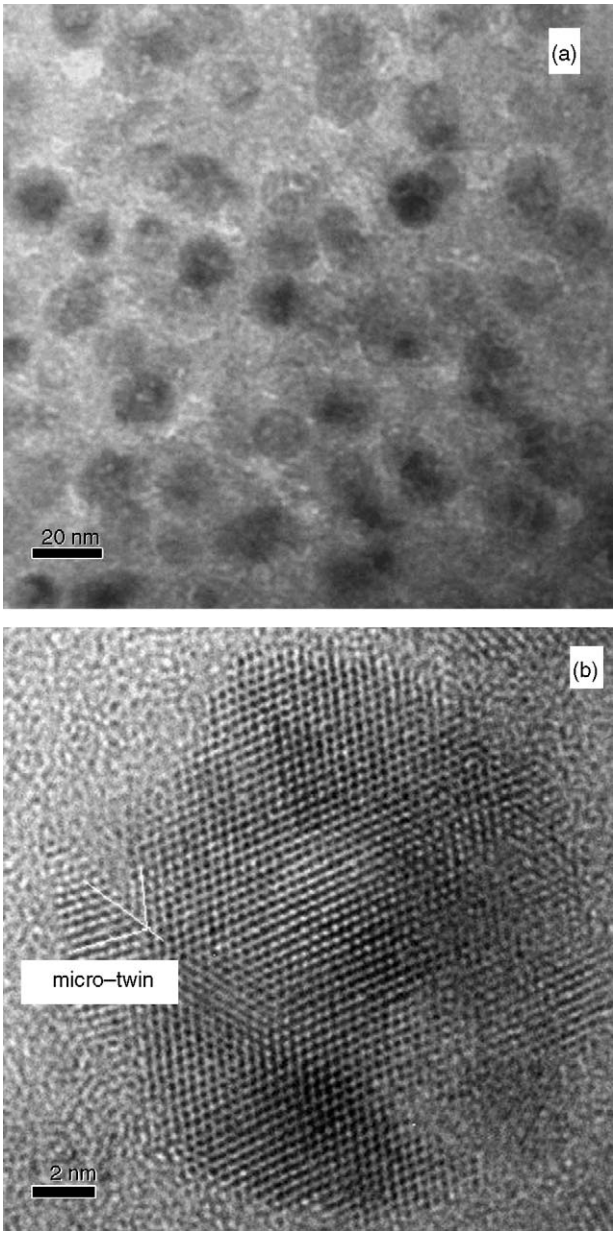


Fig. 10. TEM micrographs of sample 3 heat-treated at 670 °C. (a) Bright field image showing the distribution of $LaF_3$ crystallites, and (b) high-resolution image of a crystallite embedded in the glassy matrix.

### 3.2. XRD analysis

The typical XRD patterns for the sample 3 in the state of as-made and heat-treated at 650 °C respectively are shown in Fig. 5. For the as-made sample it exhibited typical amorphous feature, while for the heat-treated sample several hexagonal $LaF_3$ crystalline peaks emerged from the glassy hump, indicating the crystallization of $LaF_3$ from the glass matrix.

The lattice parameters of $LaF_3$ crystalline phase were evaluated from the position of XRD peaks, and are shown in Fig. 6 as a function of $NdF_3$ content. Obviously, both *a* and *c* decrease slightly but monotonously with increasing of $Nd^{3+}$ doping. Since the radius of $Nd^{3+}$ ions (0.0995 nm) is smaller than that of $La^{3+}$ ions (0.1061 nm), it may be due to

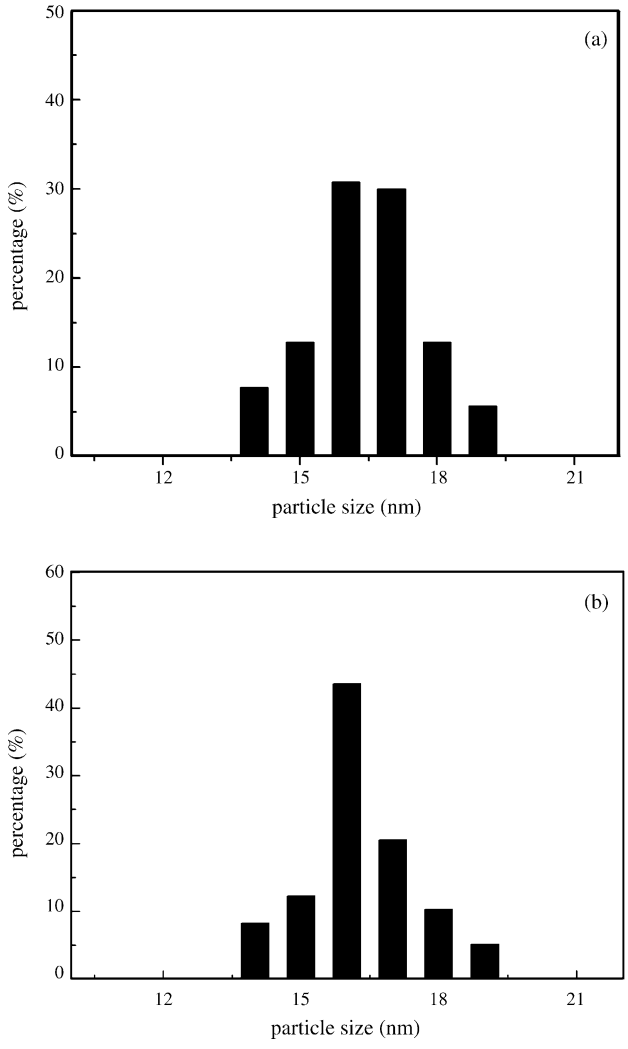


Fig. 11. The histograms based on TEM observations showing crystalline size distributions of (a) sample 1, and (b) sample 3.

the incorporation of $Nd^{3+}$ ions into the $LaF_3$ lattices by partially substituting $La^{3+}$. With increasing substitution of $Nd^{3+}$ for $La^{3+}$, more lattice shrinkage was resulted.

From the XRD peaks width and Scherrer equation, the mean sizes of $LaF_3$ crystallites for different samples were estimated and plotted as a function of $NdF_3$ content in Fig. 7. The mean crystallite size was almost the same when $NdF_3$ content is low ($\leq$1 mol%). It abruptly increased for about 35% when doping lever was adjusted from 1 to 2 mol% and further higher. It is remarkable that the evolutions of the mean crystallite size and the crystallization activation energy versus the doping lever are closely related. A decrease in $E$ means the reducing of barrier for crystallization, indicating that the samples with higher $NdF_3$ content are more susceptible to crystallize,[18] which explains why the high-doped samples had larger crystalline size after the identical thermal treatment.

### 3.3. TEM observation

The TEM bright field image and the corresponding electron diffraction pattern of the as-made sample 3 are shown in Fig. 8, demonstrating a typical glassy structure. TEM images for samples 1 and 3 heat-treated at 670 °C are presented in Fig. 9(a) and Fig. 10(a), respectively, showing many spherical crystallites precipitated homogeneously from the glass matrix. The particle size distribution for samples 1 and 3 is shown by the histogram in Fig. 11, which reveals that the crystallites are mostly sized 16–17 nm. Compared to the case for $NdF_3$ free sample, the number density of crystallites in sample 3 is relatively higher with their size remains almost unchanged. HRTEM images reveal the detailed lattice structure of individual $LaF_3$ crystallite, as shown in Fig. 9(b) and Fig. 10(b). It is noted that there are some lattice defects, e.g. micro-twins, existed inside the nano-crystallites.

The EDS spectra with nano-sized probe obtained from the glass matrix and from the crystallite shown in Fig. 10(b) are exhibited in Fig. 12. The spectrum of the glass matrix shows high content of Si, Al, the relatively weak La peaks are due to existing of $LaF_3$ clusters in glass matrix or contaminating from the $LaF_3$ crystallites. The Nd concentration is under detecting limit. As a comparison, the spectrum from the crystallite is rich in La and Nd, the weak Al, Si peaks are due to contamination from the glass matrix, indicating that $Nd^{3+}$ ions concentrated mainly inside the crystallites.

### 3.4. Absorption spectrum

The changes of the $Nd^{3+}$ site environmental structure as the result of host transition from glass to glass-ceramics may cause the difference in optical spectroscopy. The absorption spectra of the $Nd^{3+}$ ions of the sample 3 in as-made state and heat-treated state are exhibited in Fig. 13. It is evident that for the crystallized sample the absorption band centers shift to

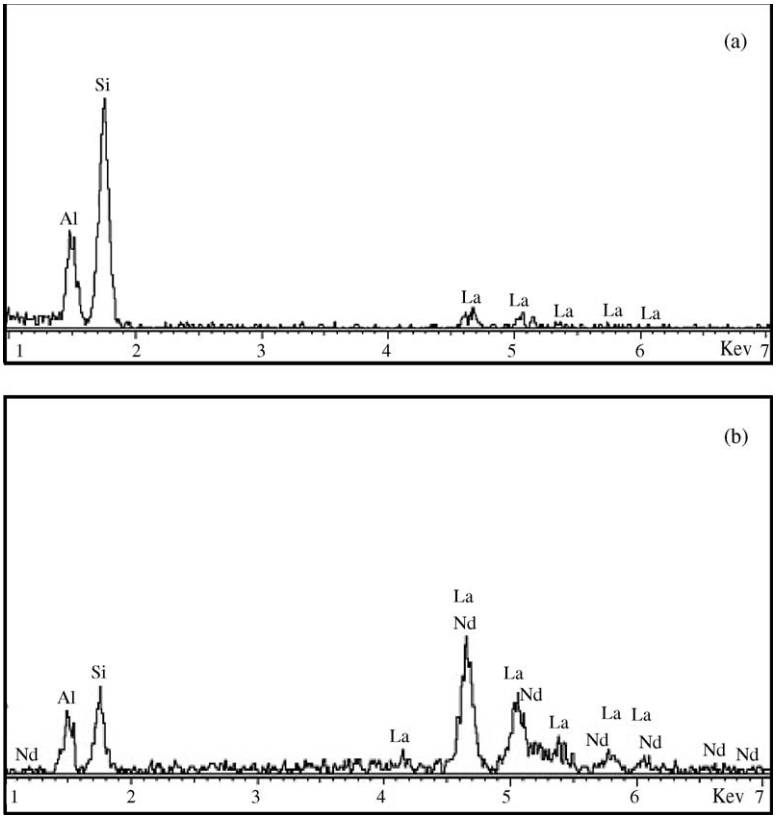


Fig. 12. EDS spectra of sample 3: (a) from glass matrix, and (b) from the crystallite shown in Fig. 10(b).

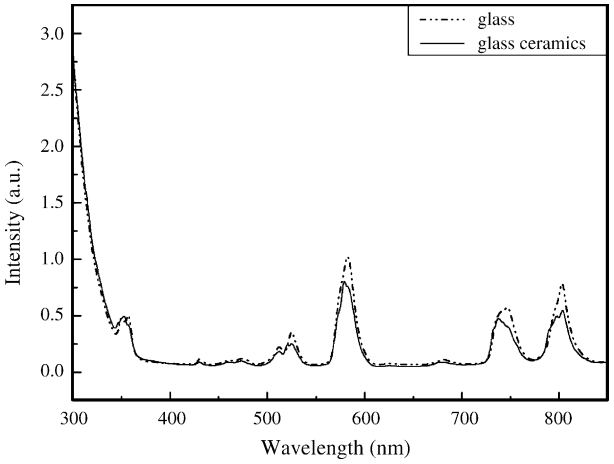


Fig. 13. Room temperature absorption spectrum of sample 3 in the states of as-made and heat-treated at 650 °C, respectively.

lower wavelength side, and more resolved Stark components of the band are obtained. The band shift and Stark splitting are the signs for the transformation of environmental structure of $Nd^{3+}$ site from amorphous to ordered crystalline, which confirms the incorporation of $Nd^{3+}$ ions into $LaF_3$ crystallites during crystallization.

## 4. Conclusion

The crystallization kinetics was studied for $41.2SiO_2$-$29.4Al_2O_3$-$17.6Na_2CO_3$-$11.8LaF_3$ glass samples with different $NdF_3$ doping. After thermal treatment, only hexagonal $LaF_3$ nano-phase crystallized from the glass matrix in a mechanism of diffusion-controlled growth process with zero nucleation rate. The doped $Nd^{3+}$ ions incorporated into the $LaF_3$ crystals resulting in the shrinkage of the lattice. Besides, they played the role as nucleating agent producing a downshift of crystallization temperature. The crystallization activation energy and the size of crystallites are also affected by doping of $NdF_3$.

## Acknowledgements

This work was supported by grants from the Natural Science Foundation of Fujian Province China (project no A0320001), the Ministry of Science and Technology of China (project no. 2003BA323C) and the State Key Laboratory of Structural Chemistry of China (project no. 050005).

## References

1. Wang, Y. and Ohwaki, J., New transparent vitroceramics codoped with $Er^{3+}$ and $Yb^{3+}$ for efficient frequency upconversion. *Appl. Phys. Lett.*, 1993, **63**(24), 3268–3270.
2. Goutaland, F., Jander, P., Brockleshy, W. S. and Dei, G., Crystallization effects on rare earth dopants in oxyfluoride glass ceramics. *Opt. Mater*, 2003, **22**(4), 383–390.
3. Johnson, L. F. and Ballman, A. A., Coherent emission from rare earth ions in electro-optic crystals. *Appl. Phys.*, 1969, **40**(1), 297–302.
4. Badzjak, J., Chizhov, S. A., Kozlov, A. *et al.*, Picosecond, terawatt, all-Nd:glass CPA laser system. *Opt. Commu.*, 1997, **134**(1–6), 495–502.
5. Mortier, M. and Vivien, D., Ceramic and glass-ceramic lasers. *Ann. Chim Sci. Mater*, 2003, **28**, 21–33.
6. Kang, U. K., Chuvaeva, T. L., Onushchenko, A. A. *et al.*, Radiative properties of Nd-doped transparent glass-ceramics in the lithium aluminosilicate system. *J. Non-Cryst. Solids*, 2000, **278**(1–3), 75–84.
7. Duan-Mu, Q. D., Su, C. H. and Wang, Y., Transparent glass-ceramics doped by $Cr^{3+}$ and $Nd^{3+}$. *J. Changchun Inst. Opt. Fine Mech.*, 1995, **18**(1), 15–18.
8. Abril, M., Mendez-Ramos, J., Martin, I. R. *et al.*, Optical properties of $Nd^{3+}$ ions in oxyfluoride glasses and glass ceramics comparing different preparation methods. *J. App. Phy.*, 2004, **95**(10), 5271–5279.
9. Malthew, J. and Dejneke, The luminescence and structure of novel transparent oxyfluoride glass-ceramics. *J. Non-Cryst. Solids*, 1998, **239**(1–3), 149–155.
10. Tanabe, S., Hayashi, H., Hanada, T. and Onodera, N., Fluorescence properties of $Er^{3+}$ ions in glass ceramics containing $LaF_3$ nanocrystals. *Opt. Mater*, 2002, **19**(3), 343–349.
11. Zarzycki, J., *Les verres et 1′ étal vitreux*. Masson, Paris, 1982, p. 47.
12. Christian, J. W., *The theory of transformations in metals and alloys* (*2nd ed.*). Pergamon Press, Oxford, 1975.
13. Brown, M. E. and Galwey, A. K., The distinguishability of selected kinetic models for isothermal solid-state reactions. *Therm. Chim. Acta*, 1979, **29**(1), 129–146.
14. Ozawa, T., Kinetics of non-isothermal crystallization. *Polymer*, 1971, **12**(3), 150–158.
15. Málek, J., Kinetic analysis of crystallization process in amorphous materials. *Therm. Chim. Acta*, 2000, **355**(1–2), 239–253.
16. Christian, J. W., *The theory of Transformation in Metals and alloys* (*2nd ed.*). Pergamon, Oxford, 1975.
17. Silva, M. A. P., Briois, V., Poulain, M. *et al.*, $SiO_2$–$PbF_2$–$CdF_2$ glasses and glass ceramics. *J. Phys. Chem. Sol.*, 2003, **64**(1), 95–105.
18. Henry, J. and Hill, R. G., The influence of lithia content on the properties of fluorphlogopite glass-ceramics. I. Nucleation and crystallisation behaviour. *J. Non-Cryst. Solids*, 2003, **319**(1/2), 1–12.